512 *Biochemistry* **2011,** *50,* 512–522
DOI: 10.1021/bi1013563

BIOCHEMISTRY
including biophysical chemistry & molecular biology
Article

Interaction between CK2α and CK2*β*, the Subunits of Protein Kinase CK2: Thermodynamic Contributions of Key Residues on the CK2α Surface[†]

Jennifer Raaf,[‡,∥] Nils Bischoff,[‡] Karsten Klopffleisch,[‡] Elena Brunstein,[‡] Birgitte B. Olsen,[§] Greg Vilk,[∥] David W. Litchfield,[∥] Olaf-Georg Issinger,[§] and Karsten Niefind*[,‡]

[‡]*Department für Chemie, Institut für Biochemie, Universität zu Köln, Zülpicher Str. 47, D-50674 Köln, Germany,* [§]*Institut for Biokemi og Molekylær Biologi, Syddansk Universitet, Campusvej 55, DK-5230 Odense, Denmark, and* [∥]*Department of Biochemistry, Schulich School of Medicine and Dentistry, University of Western Ontario, London, Ontario, Canada N6A 5C1*

Received August 22, 2010; Revised Manuscript Received November 26, 2010

ABSTRACT: The protein Ser/Thr kinase CK2 (former name: casein kinase II) exists predominantly as a heterotetrameric holoenzyme composed of two catalytic subunits (CK2α) bound to a dimer of noncatalytic subunits (CK2*β*). We undertook a study to further understand how these subunits interact to form the tetramer. To this end, we used recombinant, C-terminal truncated forms of human CK2 subunits that are able to form the holoenzyme. We analyzed the interaction thermodynamics between the binding of CK2α and CK2*β* as well as the impact of changes in temperature, pH, and the ionization enthalpy of the buffer using isothermal titration calorimetry (ITC). With structure-guided alanine scanning mutagenesis we truncated individual side chains in the hydrophobic amino acid cluster located within the CK2α interface to identify experimentally the amino acids that dominate affinity. The ITC results indicate that Leu41 or Phe54 single mutations were most disruptive to binding of CK2*β*. Additionally, these CK2α mutants retained their kinase activity. Furthermore, the substitution of Leu41 in combination with Phe54 showed that the individual mutations were not additive, suggesting that the cooperative action of both residues played a role. Interestingly, the replacement of Ile69, which has a central position in the interaction surface of CK2α, only had modest effects. The differences between Leu41, Phe54, and Ile69 in interaction relevance correlate with solvent accessibility changes during the transition from unbound to CK2*β*-bound CK2α. Identifying residues on CK2α that play a key role in CK2α/CK2*β* interactions is important for the future generation of small molecule drug design.

The function of eukaryotic protein kinases (EPKs)[1] to operate as molecular switches in signal transduction pathways of the cell is profoundly interconnected with their ability to undergo reversible protein/protein interactions either with regulatory subunits, which ensure their strictly controlled activity, or with up- and downstream components of signaling cascades.

EPKs play an important role in various pathologies such as cancer and hence are regarded as valuable targets for pharmacological inhibition. Most EPK inhibitors are ATP-competitive, a strategy, which although successful in many cases, has the disadvantage that the ATP-binding pockets of different protein kinases are fairly similar. Therefore, efforts have been made in the last years to design molecules that disrupt protein/protein interactions and to "jump out of the catalytic box" (*1*) to overcome selectivity problems of ATP-competitive inhibitors and to exploit the ability of protein kinases to associate with regulatory or substrate proteins.

At first glance, addressing protein/protein interaction surfaces is a challenging task because in most cases these surfaces are large and therefore a difficult target for small-molecule interference. However, by looking at the individual residues within interaction interfaces of proteins, it appears that the energy of binding is not evenly distributed but rather due to a limited subset of residues (*2*). For the rational development of small molecules that prevent association, detailed knowledge of these energetic hot spots is required.

The subject of the present study is protein kinase CK2, a classical protein serine/threonine kinase implicated in disease (*3*) for which many ATP-competitive inhibitors are known (*4*). However, as is the case with many ATP-competitive kinase inhibitors, these CK2 inhibitors exhibit off-target effects (*5*). To overcome these limitations, the distinctive quaternary structure of CK2 (ref *6*, Figure 1A) raises the prospect of modulating CK2 by systematically interfering with the assembly of its subunits.

The catalytic CK2α subunit is a member of the CMGC group of eukaryotic protein kinases; i.e., it is closely related to the cyclin-dependent kinases, the mitogen-activated kinases, and glycogen synthase kinase 3. However, while those kinases are strictly regulated, CK2α is constitutively active, meaning none of

[†]This work was supported by the Danish Research Council (Grant 21-01-0511), the Deutsche Forschungsgemeinschaft (Grant NI 643/1-3), the Fritz-Thyssen-Stiftung (Grant 40.09.0.033), and the Canadian Institutes of Health Research (Grant MOP 37854).

*To whom correspondence should be addressed. E-mail: Karsten.Niefind@uni-koeln.de. Telephone: +49 221 4706444. Fax: +49 221 4706431.

[1]Abbreviations: ASA, accessible surface area, BSA, bovine serum albumin; EPK, eukaryotic protein kinase; CMGC, subgroup of the eukaryotic protein kinases denoted after the cyclin-dependent kinases, the mitogen-activated kinases, glycogen synthase kinase 3, and the cell division control 2-like kinases; ITC, isothermal titration calorimetry; DSC, differential scanning calorimetry; DTT, dithiothreitol; GST, glutathione *S*-transferase; TBST, Tris-buffered saline with Tween 20.

 Published on Web 12/13/2010

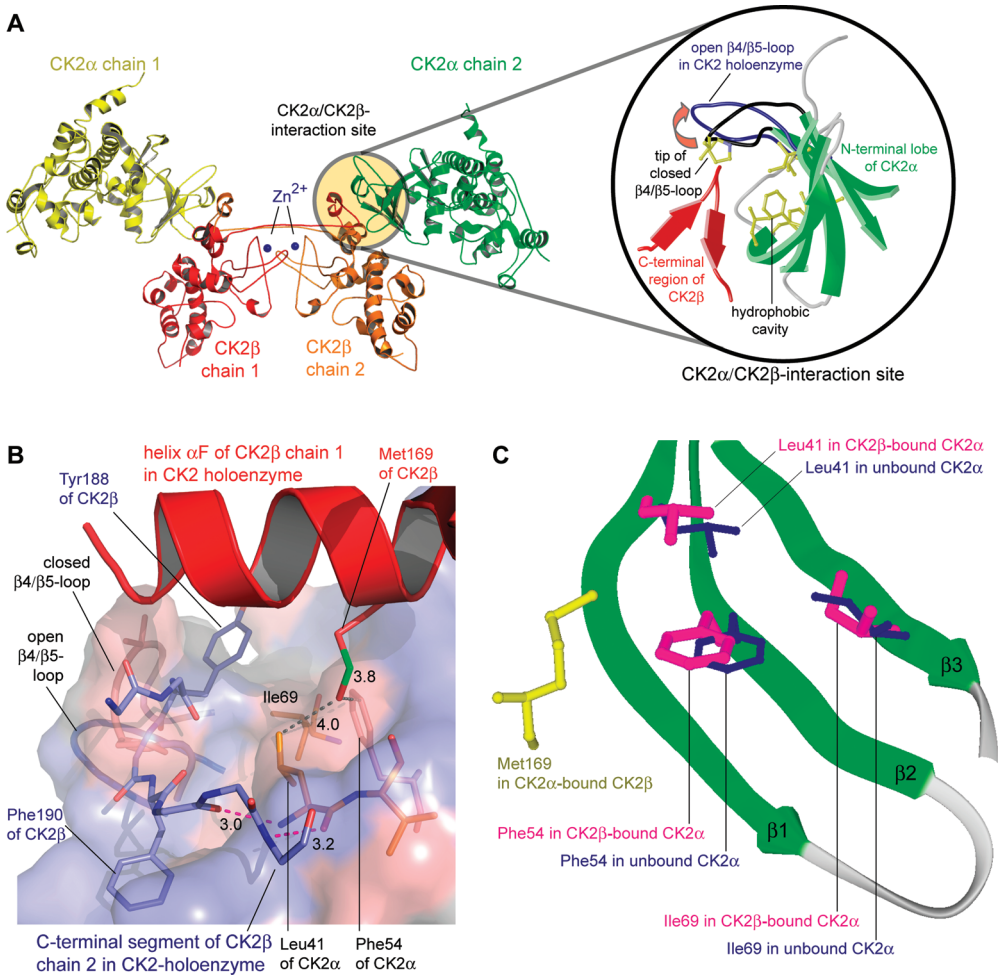

FIGURE 1: Structural background of the CK2α/CK2β interaction study. (A) Crystal structure of the CK2 holoenzyme (*6*). The zoom area illustrates details of the CK2α/CK2β interaction site, in particular various hydrophobic side chains at the outer surface of the central β-sheet of the N-terminal CK2α domain and a characteristic motion of the β4/β5 loop that opens upon CK2 holoenzyme formation. The picture was drawn with BOBSCRIPT (*39*) and RASTER3D (*40*). (B) Surface representation of the CK2α/CK2β contact. Hydrophobic surface areas are colored red; hydrophilic areas are colored blue. Important structural elements of the CK2β subunit are emphasized. Exchanged residues of CK2α and the residues at the tip of the β4/β5 loop are drawn as sticks. Distances are given in Å. The picture was drawn with PYMOL (*41*). (C) The three modified residues of this study on top of three different β-strands of human CK2α. The β-strands and the blue versions of Leu41, Phe54, and Ile69 are drawn from a high-resolution 3D structure of monomeric $CK2\alpha^{1-335}$ (*37*). The magenta version of the side chains as well as Met169 of CK2β (yellow) is extracted from the CK2 holoenzyme structure (*6*) after structural superimposition of the CK2α subunits. The picture was created with BRAGI (*42*).

the conventional regulation mechanisms such as (de)phosphorylation, second messenger binding, or the binding or release of regulatory subunits apply (*7*). In particular, CK2β is not an on/off switch of CK2α but a modulator of its substrate specificity and a stabilizator against denaturing forces (*8*, *9*).

The value of CK2 as a pharmacological target arises from its relation to many human diseases (*3*), in particular to cancer. CK2 does not initiate tumorigenesis, but an increased CK2 activity is observed in a wide variety of tumors (*3*). It contributes to a cellular environment conducive to the tumor phenotype (*10*). In this respect, tumors benefit from the antiapoptotic function of CK2 (*11*−*13*). For example, the CK2-catalyzed phosphorylation of the tumor suppressor PML leads to proteasomal degradation of PML (*14*). Additionally, CK2 plays a role in the development of the multidrug resistance phenotypes in cancers that have been treated by chemotherapy (*15*, *16*).

While both CK2α and the CK2 holoenzyme are catalytically active *in vitro*, it remains unclear which is the more important entity in cells. A recent study suggests that the cellular CK2 activity might be almost entirely due to the holoenzyme (*17*), an observation that is consistent with the high stability of the complex [dissociation constant between 3.7 nM (this study) and 5.4 nM (*18*)]. By comparison, *in vivo* imaging results show that both CK2α monomers and CK2β dimers can move independently in living cells (*19*), a result that correlates well with the crystallographic finding that the CK2α/CK2β interface size 832 $Å^2$ (*6*) is in the typical range found for nonobligate complexes. In any case the strong impact of CK2β on the stability and the enzymological profile of CK2α encourages the development of molecules that either prevent the association of the subunits or induce their dissociation and thereby affect the phosphorylation of CK2β-dependent substrates (*20*).

To enable the development of small molecules that modulate assembly of CK2 complexes, structural and biophysical information about the CK2α/CK2β interaction is required. Structure determinations of the human CK2 holoenzyme (ref *6*, Figure 1A) and of the unbound forms (isolated human CK2α and CK2β) provided substantial knowledge about the nature and location of the interaction site on the surface of either CK2α or CK2β and about conformational changes associated with the assembly.

Those studies revealed that CK2β dimers use both chains to form a convex interface (Figure 1A) fitting to a concave and hydrophobic pendant on the surface of CK2α, more precisely on the outer surface of the central β-sheet within the N-terminal domain (ref *6*, Figure 1C). While the CK2β dimers are structurally preformed for the interaction, CK2α undergoes a large conformational adaptation in the β4/β5 loop (zoom area of Figure 1A) that opens such that the hydrophobic surface becomes accessible for CK2β.

There are indications that small molecules can enter this region of CK2α even with a closed β4/β5 loop. In this case a relatively small hydrophobic pocket is formed that can harbor certain compounds (*20*, *21*). These and other molecules (*22*) that were shown directly to interfere with the CK2α/CK2β interaction can serve as lead structures for the development of CK2β antagonists. The potential utility of these molecules is further enhanced since non-ATP-competitive inhibition of CK2α was observed in addition to their impact on the CK2α/CK2β interaction (*22*).

As outlined above, knowledge about the "hot spots" of a protein/protein interaction is particularly relevant for a detailed understanding as well as the design of antagonists. In the case of the CK2α/CK2β contact the CK2β side is relatively well investigated since Laudet and co-workers (*20*) revealed that Tyr188 and Phe190 in the C-terminal region of CK2β (Figure 1B) are essential side chains for the interaction with CK2α, a finding which led to structure-based design of CK2β antagonizing peptides (*20*).

To complement those studies, we describe here a thorough investigation of the CK2α side of the interaction and the identification of energetic "hot spots" on the surface of CK2α. For this purpose we used structure-guided alanine scanning mutagenesis combined with isothermal titration calorimetry, which allows the direct measurement of the thermodynamic parameters of the binding reaction. Additionally, the CK2α mutants created in this context were characterized regarding thermostability and catalytic activity in comparison to the wild type in order to identify CK2α mutants with impaired affinity to CK2β but in other respects wild-type properties.

EXPERIMENTAL PROCEDURES

Mutagenesis. The gene sequence of the CK2α subunit from *Homo sapiens* was used to prepare the point mutants using the Quik Change site-directed mutagenesis kit (purchased from Stratagene). The wild-type protein of human CK2α (EC 2.7.11.1; CSNK2A1) consists of 391 amino acids (NCBI reference sequence number: NG_011970.1) and occurs in all human tissues. The CK2α wild type is less stable under *in vitro* conditions than the C-terminal deletion mutant CK2α$^{1-335}$ (*23*) utilized in the calorimetric measurements of this study. As an interaction partner we took the mutant CK2β^{1-193}, the construction and characterization of which was described by Boldyreff et al. (*24*). For the purpose of an *in vitro* pull-down assay N-terminal GST-fused, full-length CK2α and CK2α variants were applied.

The sequences of primers for the Leu41Ala mutation were 5′-GAAATCAAGATGACTACCAG**GCG**GTTCGAAAATTAGGCCGAG-3′ (sense primer) and 5′-CTCGGCCTAATTTTCGAAC**CGC**CTGGTAGTCATCTTGATTTC-3′ (antisense primer).

The primers for the Phe54Ala mutation had the following sequences: 5′-TAGGCCGAGGTAAATACAGTGAAGTA**GCT**GAAGCCATCAACATC-3′ (sense primer) and 5′-GATGTTGATGGCTTC**AGC**TACTTC;ACTGTATTTACCTCGGCCTA-3′ (antisense primer).

The sequences of primers to create the Ile69Ala mutation were 5′-GCCATCAACATCACAAATAATGAAAAAGTTGTTGTTAAA**GCT**CTCAAGCCAGTAAAAAAGA-3′ (sense primer) and 5′-TCTTTTTTACTGGCTTGAG**AGC**TTTAACAACAACTTTTTCATTATTTGTGATGTTGATGGC-3′ (antisense primer).

The Leu41Ala/Phe54Ala double mutant was created with the following primers on the basis of the Phe54Ala point-mutated plasmid: 5′-GAAATCAAGATGACTACCAG**GCG**GTTCGAAAATTAGGCCGAG-3′ (sense primer) and 5′-CTCGGCCTAATTTTCGAAC**CGC**CTGGTAGTCATCTTGATTTC-3′ (antisense primer).

The positions of the exchanged codons are shown in bold. All constructs were verified by DNA sequencing.

The expression vectors were either pT7-7 for the CK2α$^{1-335}$ and CK2β^{1-193} constructs or pGEX-KG-tev for the GST-tagged CK2α constructs. For the expression of His-tagged CK2β a pET28A vector with the full-length CSNK2B gene (NCBI reference sequence number: NM_001320.5) was used.

Protein Expression and Purification. All proteins were recombinantly expressed in *Escherichia coli* BL21(DE3) cells. The *E. coli* BL21(DE3) cells harboring the different plasmids were grown to an OD_{600} of 0.6−0.8 in LB media containing 50 μg/mL ampicillin. ITPG at a final concentration of 0.5 mM was supplemented to induce protein expression. This culture was then grown for a further 3 h with shaking at 30 or 37 °C. The cells were ultimately collected, washed, and then lysed using a French press or using 150 mM NaCl, 50 mM Tris-HCl, pH 7.5, 1 mM DTT, 0.5 mM EDTA, 0.5% Triton X-100, and protein inhibitors such as PMSF and aprotinin. Cellular debris was removed by centrifugation.

The first purification step for the CK2α$^{1-335}$ variants and CK2β^{1-193} was performed using phosphocellulose chromatography. The column was equilibrated with 300 mM NaCl and 25 mM Tris-HCl, pH 8.5. After protein application and washing a gradient elution was performed using 1 M NaCl and 25 mM Tris-HCl, pH 8.5, as high-salt component. For the CK2α$^{1-335}$ variants the second purification step was affinity chromatography with a HiTrap heparin HP column (GE HealthCare). The equilibration and low-salt solution of the gradient was 400 mM NaCl and 25 mM Tris-HCl, pH 8.5, and the high-salt component was 1 M NaCl and 25 mM Tris-HCl, pH 8.5. The second step for CK2β^{1-193} was an anion-exchange chromatography with a HiTrap Sepharose Q column (GE HealthCare). The equilibration and low-salt solution of the gradient was 150 mM NaCl and 25 mM Tris-HCl, pH 8.5, and the high-salt component was 1 M NaCl and 25 mM Tris-HCl, pH 8.5. The purity of the protein was verified by SDS−PAGE.

Finally, the proteins were concentrated and rebuffered in 500 mM NaCl and 25 mM Tris-HCl, pH 8.5, by ultrafiltration using AMICON Ultra-15 tubes. During this step the double mutant CK2α$^{1-335,Leu41Ala,Phe54Ala}$ suffered from serious solubility problems; the maximum concentration for this mutant was 21 μM corresponding to 0.84 mg/mL. Moreover, the stability of this mutant was limited as observable from a degradation band around 25 kDa on lane 11 of Figure 4B.

The GST-tagged CK2α variants were purified using glutathione−agarose beads (Sigma). The cleared cell lysate was incubated for 1 h with the glutathione−agarose beads at 4 °C upon which they were loaded in a Bio-Rad disposable column. The column

was washed with high salt (i.e., 1 M NaCl) to remove nonspecific proteins. Finally, the glutathione−agarose beads containing purified GST-CK2α were reequilibrated in 150 mM NaCl, 1 mM DTT, 0.5 mM EDTA, 50 mM Tris-HCl, pH 7.5, and 50% glycerol and stored at −20 °C until further use.

The His-tagged CK2β subunit was purified using Ni-NTA beads (Qiagen) as per the manufacturer's instructions. Briefly, the protein was expressed similarly as described above. When the His-CK2β was captured on Ni-NTA beads, it was then eluted using 1 M imidazole, 150 mM NaCl, 50 mM Tris-HCl, pH 7.5, and added protease inhibitors. His-CK2β was then dialyzed with decreasing imidazole concentrations in the dialysis buffer (400 mM NaCl, 1 mM EDTA, 1 mM DTT, 0.05% Triton X-100, 10% glycerol, 50 mM Tris-HCl, pH 8.0, and added protease inhibitors) until imidazole was removed and stored at −80 °C until later use.

Analytical Gel Filtration. Mixtures of human CK2β^{1-193} and each of the human CK2α^{1-335} variants were applied to an analytical gel filtration column (10/300 GL Superdex 200 from GE HealthCare) that had been equilibrated with 500 mM NaCl and 25 mM Tris-HCl, pH 8.5. In each run the protein sample applied to the column had a volume of 500 μL, a CK2β^{1-193} concentration of 12 μmol/L, and a molar concentration of the respective CK2α variant that was at least twice as much. The column was calibrated with L-lactate dehydrogenase from pig heart (146 kDa), bovine serum albumin (66.4 kDa), and hen egg white lysozyme (14.6 kDa). All gel filtration runs were performed at 10 °C.

Enzyme Kinetics. The enzymatic activity of the purified CK2α^{1-335} variants was determined with a continuous, coupled *in vitro* assay (*25*). The equations of the coupled reactions are the following: (i) reaction catalyzed by CK2α, casein + ATP → phosphorylated casein + ADP; (ii) coupled reaction catalyzed by pyruvate kinase, ADP + phosphoenolpyruvate → pyruvate + ATP; (iii) detectable reaction catalyzed by lactate dehydrogenase, pyruvate + NADH + H^+ → lactate + NAD^+.

The assay was performed at 20 or 30 °C under atmospheric pressure. For 20 °C a pH of 8.48 and for 30 °C a pH of 8.40 were measured without adding the CK2α^{1-335} variant. As CK2α substrate casein (purchased from Sigma) was present in the reaction at a concentration of 3 mg/mL. To solve casein in the stock solution (5 mg/mL), NaOH was added, and the solution was liberated from impurities by filtration. Additionally, the assay mixture contained 20 mM $MgCl_2$, 100 mM Tris-HCl, pH 8.3 (reaction buffer), 0.02 mg/mL CK2α^{1-335} variant, 1 mM phosphoenolpyruvate, 5 μg/mL lactate dehydrogenase (Roche), 5 μg/mL pyruvate kinase (Roche), and 0.2 mM NADH. The cosubstrate ATP, solved in the reaction buffer, was varied in the range of 10−200 μM. Initial rates of the reaction were measured by the slope of decreasing absorption at 340 nm, caused by NAD^+ formation. The proportionality between the initial velocity and the CK2α^{1-335} concentration was checked at 30 °C to ensure that the casein phosphorylation reaction was rate-limiting. Each data point was measured three times, and the mean and standard deviation were calculated. Michaelis−Menten parameters were determined with GraFit 4.0 (Erithacus Software, Horley, U.K.).

DSC Measurements. For DSC data collection a VP-DSC (MicroCal, Northampton, MA, USA) was used. For every protein three temperature scans were performed from 20 to 80 °C at a scan rate of 25 °C/h. The protein concentrations varied between 55 and 100 μM for the CK2α^{1-335} variants. In all cases the protein buffer was 500 mM NaCl and 25 mM Tris-HCl, pH 8.5. In the case of the double mutant CK2$\alpha^{1-335,Leu41Ala,Phe54Ala}$ the highest concentration we could achieve (21 μM), in particular combined with a decrease of solubility with increasing temperature, was too low to obtain a DSC curve. Processing of the raw data was performed with the ORIGIN software (version 7), Origin Lab, Northampton, MA, USA.

ITC Measurements. All experiments were performed with a VP-ITC (MicroCal, Northampton, MA, USA) at a temperature range between 20 and 35 °C. Protein concentrations were determined by absorbance. CK2β^{1-193} was provided in the sample cell at concentrations between 9 and 20 μM. CK2α^{1-335} was present in the injection syringe at concentrations between 80 and 200 μM. In the case of the double mutant CK2$\alpha^{1-335,Leu41Ala,Phe54Ala}$ the low concentration of 21 μM enforced an inversion of the experimental setup: here CK2$\alpha^{1-335,Leu41Ala,Phe54Ala}$ was placed into the sample cell at 17−21 μM, CK2β^{1-193} was present in the syringe at 172 μM, and the option "ligand in cell" was chosen for evaluation.

Both proteins were diluted in buffers containing 500 mM NaCl and variable buffer substances (25 mM Tris-HCl, 25 mM HEPES, or 25 mM PIPES) to the required concentrations and subsequently degassed. The pH of the Tris-HCl buffer was varied between pH 7.4 and pH 9.0. Each ITC experiment consisted of one initial injection of 2 μL followed by 24 injections of 10 μL. The injections were made over a period of 20 s with a 300 s interval between subsequent injections.

The raw ITC data (Figure 3A−E, upper panels) were processed with the ORIGIN software (version 7), Origin Lab, Northampton, MA, USA, assuming a binding model of a single set of two equivalent sites (meaning two CK2α^{1-335} ligands bind to one CK2β^{1-193} dimer). The final values (Table 1) are averages of three repetitions.

In Vitro Pull-Down Assay with Immunoblot Analysis. Glutathione−agarose beads with coupled GST-tagged CK2α variants and GST without CK2α were diluted 1:100 in 150 mM NaCl, 1 mM DTT, 0.5 mM EDTA, and 50 mM Tris-HCl, pH 7.5. The diluted beads (10−50 μL, to achieve equal amounts of the coupled proteins) were incubated for 1 h with shaking at 4 °C with 2.4, 1.2, and 0.12 μg/mL of His-tagged CK2β in 500 μL of detergent buffer [1% (v/v) Nonidet P-40, 1% (w/v) deoxycholic acid, 0.5% (w/v) SDS, 150 mM NaCl, 1 mM DTT, 0.5 mM EDTA, 50 mM Tris-HCl, pH 7.5, with added protease inhibitors]. The beads were then washed four times with 1 mL of detergent buffer, and then 50 μL of Laemmli buffer was added to release GST or CK2 proteins from the beads. These proteins were loaded onto 12% SDS−PAGE gels, electrophoresed for 1 h at 200 V, and then transferred to a polyvinylidene difluoride (PVDF) membrane (Boeringer Mannheim) using a Trans-blot Semi Dry Electrophoretic transfer apparatus (purchased from Bio-Rad). We proceeded to immunoprobe the membrane with antibodies specific for GST and human CK2β. First, the PVDF membrane was blocked for 1 h with 5% BSA in TBST; then, mouse anti-GST (Sigma) and rabbit anti-CK2β in 1% BSA/TBST were added together at concentrations of 1:10000 and 1:25000, respectively. After extensive washes with TBST, the CK2 proteins were visualized using fluorophore-linked secondary antibodies such as goat anti-mouse (GAM, 680 nm) and goat anti-rabbit (GAR, 800 nm) antibodies obtained from LI-COR Biosciences. Fluorescence was detected and quantified using a LI-COR near-infrared fluorescent scanner and processed using Odyssey V3.0 software.

Table 1: Alanine Scan Thermodynamic Parameters[a]

mutant	$\Delta G°$ (J/mol)	$\Delta H°$ (J/mol)	$\Delta S°$ [J/(mol·K)]	$K_D = K_A^{-1}$ (nmol/L)	$\Delta\Delta G°$ (J/mol)
CK2α$^{1-335}$ (wt)	−47303 ± 928	−63833 ± 2259	−56.51 ± 5.38	3.69 ± 1.65	0
CK2α$^{1-335,Leu41Ala}$	−36116 ± 1173	−27111 ± 5789	30.73 ± 16.14	364.08 ± 173.03	−11188
CK2α$^{1-335,Phe54Ala}$	−36540 ± 671	−31969 ± 1586	15.60 ± 7.85	305.81 ± 92.27	−10764
CK2α$^{1-335,Leu41Ala,Phe54Ala}$	−37185 ± 559	−6880 ± 127	103.43 ± 2.15	234.74 ± 56.71	−10119
CK2α$^{1-335,Ile69Ala}$	−43988 ± 709	−68269 ± 4315	−82.87 ± 15.41	14.38 ± 4.72	−3317

[a] K_A, binding constant; K_D, dissociation constant; $\Delta H°$ and $\Delta S°$, enthalpic and entropic terms; N, stoichiometry; $\Delta\Delta G° = RT\ln(K_{A\_mutant}/K_{A\_WT})$; $T = 293$ K. Each experiment was performed three times; errors are standard deviations.

Computational Modeling of Thermodynamic Data. In order to subsequently calculate thermodynamic data of the interaction between CK2α$^{1-335}$ and CK2β^{1-193}, the structure of the CK2 holoenzyme (ref *6*; Protein Data Bank code 1JWH) was prepared by deleting the water molecules, the heteroatoms, and all atoms belonging to amino acid residues C-terminal of position 335 of CK2α and position 193 of CK2β. Afterward, the interface between CK2α$^{1-335}$ and CK2β^{1-193} was analyzed concerning the changes in the solvent-accessible surface area (ΔASA) with the program AREAIMOL from CCP4 program package (*26*). Following the practice of Perozzo et al. (*27*) the ΔASA values were subdivided on the basis of the atom types into a polar fraction ΔASA_{pol} (oxygen, nitrogen, and sulfur atoms) and an apolar fraction ΔASA_{ap} (carbon atoms). These ΔASA_{pol} and ΔASA_{ap}-values (more precisely, their averages over two independent CK2α/CK2β interfaces within the heterotetrameric CK2 holoenzyme) were used to calculate ΔC_p, $\Delta H°$, and $T\Delta S°$ values. The necessary equations depend originally on empirical relationships (*28*); we extracted them from an interaction analysis by Holdgate et al. (*29*) performed at 300 K and adapted them to 20 °C assuming a constant ΔC_p value in the corresponding temperature interval.

RESULTS

Impact of Temperature, pH, and Ionization Enthalpy of the Buffer on the CK2α/CK2β Interaction. As a followup to our recent ITC results, which revealed that the CK2α/CK2β interaction is highly exothermic and driven by a large enthalpic component (*30*), we investigated the interaction concerning temperature, pH dependence, and protonation or deprotonation events (Figure 2). The CK2β construct we used as the CK2α binding partner in these studies lacks the final 22 amino acids but nevertheless was shown to be fully capable of interacting with CK2α (*24*).

Our ITC runs at different temperatures (20, 25, 30, and 35 °C; Figure 2A) showed that both the change of standard enthalpy ($\Delta H°$) and the change of standard entropy ($\Delta S°$) are getting more negative with increasing temperature. Both contributions compensate each other and result in a stable change of the standard Gibbs energy $\Delta G°$. The mean value of K_D for all measurements was calculated as 4.65 nM. With the values for $\Delta H°$ and $\Delta S°$ at different temperatures a change of heat capacity (ΔC_p) of −1355 J/(mol·K) calculated with $d\Delta H°/dT$ and −1257 J/(mol·K) calculated with $T\,d(\Delta S°)/dT$ were determined.

Additionally, the impact of the pH of the solvent toward the CK2α$^{1-335}$/CK2β^{1-193} interaction was investigated. Therefore, the pH of the Tris buffer was varied between pH 7 and pH 9 while ITC measurements were performed at 35 °C. The resulting thermodynamic profiles (Figure 2B) showed no significant dependency in this pH range.

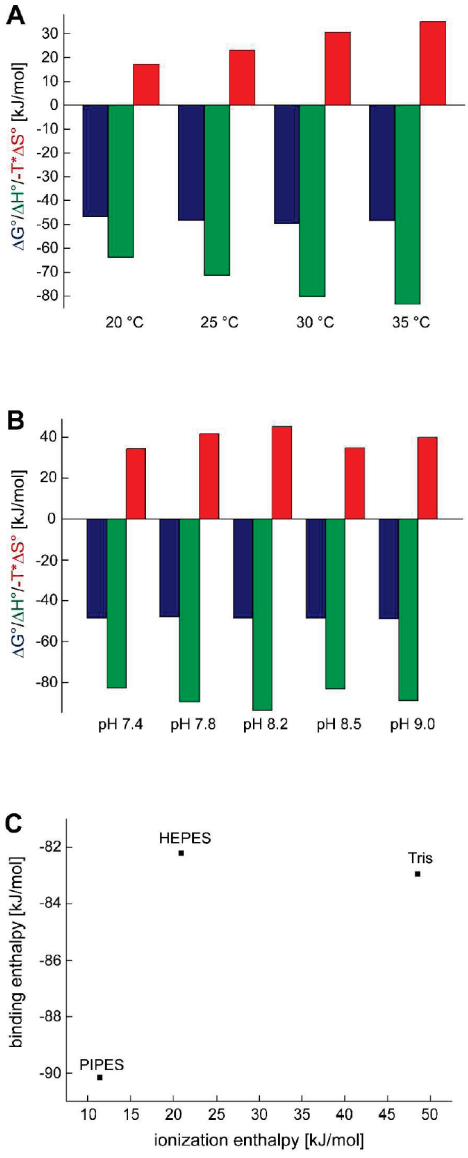

FIGURE 2: Thermodynamic characterization of the interaction between the wild-type analogue constructs CK2α$^{1-335}$ and CK2β^{1-193}. (A) Temperature dependence of the CK2α$^{1-335}$ and CK2β^{1-193} interaction. (B) pH dependence of the CK2α$^{1-335}$ and CK2β^{1-193} interaction. (C) Dependency of the CK2α$^{1-335}$ and CK2β^{1-193} association on the ionization enthalpy of the buffer. Color code: $\Delta G°$, blue; $\Delta H°$, green; $-T\Delta S°$, red.

To test if the association of the CK2 subunits is linked to an exchange of protons with the solvent, ITC experiments were performed in buffers with different ionization enthalpies [Tris, 48.50 kJ/mol; HEPES, 20.96 kJ/mol; PIPES, 11.46 kJ/mol (*31*)]. When the measured binding enthalpy is plotted against the ionization enthalpy of the buffer, the number of protonation

events occurring on complex formation can directly be determined with the slope of linear regression. Additionally, the algebraic sign of the slope indicates the direction of the transfer. In the case of the CK2α/CK2*β* interaction no linear correlation was apparent (Figure 2C), indicating that there was no significant exchange of protons during the binding reaction.

*Detection of Interaction Hot Spots in the Subunit Interface of CK2*α. To characterize the individual thermodynamic contributions and to find potential hot spots important for the interaction between CK2α and CK2*β*, several hydrophobic residues in the interaction surface of the catalytic subunit (Leu41, Phe54, Ile69, and a combination of Leu41/Phe54) were replaced by alanine.

In ITC experiments we observed in all cases heat production due to association of the CK2 subunits (Figure 3A−E). Among the single mutations, the Ile69 substitution had the least influence on the binding energy, with modest drop in affinity (K_D = 14.38 nM compared to 3.69 nM, $|\Delta\Delta G°|$ = 3.3 kJ mol^{-1}; Table 1). The entropic and enthalpic terms were both more negative compared to CK2α$^{1-335}$ but compensate to a smaller change in Gibbs energy of binding $\Delta G°$ (Figure 3E,F).

Interestingly, the replacement of Leu41 or Phe54 affected both enthalpic and entropic binding parameters and turned the entropic term favorable (Figure 3F). The characteristic entropy/enthalpy compensation was disrupted, and the driving force of the interaction, the enthalpic contribution, was reduced (27.1 kJ/mol for CK2α$^{1-335,Leu41Ala}$ and 32.0 kJ/mol for CK2α$^{1-335,Phe54Ala}$ compared to 63.8 kJ/mol for the wild-type similar CK2α$^{1-335}$; Table 1). This led to a significantly higher dissociation constant at 20 °C (K_D = 364.08 nM for CK2α$^{1-335,Leu41Ala}$ and K_D = 305.81 nM for CK2α$^{1-335,Phe54Ala}$ compared to 3.69 nM; Table 1; Figure 3B,C,F). In both cases the $|\Delta\Delta G°|$ values are larger than 2 kcal/mol (8.37 kJ/mol), which is the threshold for the definition of interaction "hot spots" introduced by Bogan and Thorn (*2*).

We decided then to produce a CK2α Leu41Ala/Phe54Ala double mutant to determine whether the binding to CK2*β* would be effectively eliminated. The ITC results for this double mutated CK2α subunit (CK2α$^{1-335,Leu41Ala,Phe54Ala}$) showed that the interaction was not completely abolished (Figure 3D). While the enthalpic contribution was substantially decreased to a value of −6.9 kJ/mol in comparison to the two single CK2α mutants,

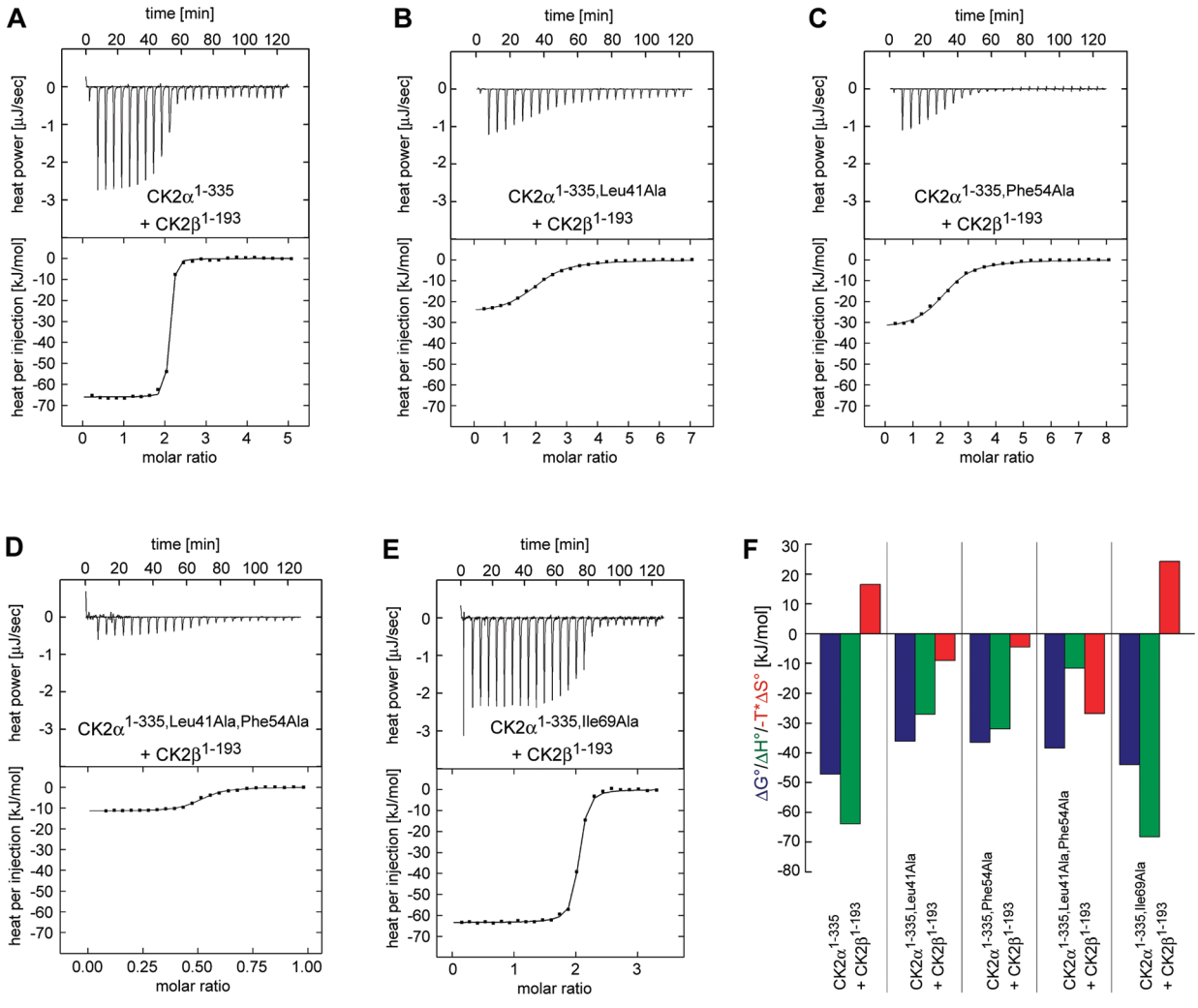

FIGURE 3: Thermodynamic characterization of the interaction of several CK2α$^{1-335}$ variants with CK2*β*$^{1-193}$. (A−F) ITC profiles of the interaction of CK2*β*$^{1-193}$ with CK2α$^{1-335}$ (A), CK2α$^{1-335,Leu41Ala}$ (B), CK2α$^{1-335,Phe54Ala}$ (C), CK2α$^{1-335,Leu41Ala,Phe54Ala}$ (D), and CK2α$^{1-335,Ile69Ala}$ (E). All ITC runs refer to 20 °C. For each interaction pair a representative example out of three ITC runs is documented. The upper halves show the original heat production upon injection and the lower ones the integrated, dilution-corrected, and normalized peaks. The final thermodynamic parameters are listed in Table 1 as average values over three repetitions. The molar ratio in panel D is according to an inverted experimental setup and the "ligand in cell" option. (F) Thermodynamic profiles derived from the ITC runs illustrated in panels A−E. Color code: $\Delta G°$, blue; $\Delta H°$, green; $-T\Delta S°$, red.

the Leu41Ala/Phe54Ala double substitution resulted in a more favorable entropy change [103.4 J/(mol·K)] that offsets and even overcompensates for the enthalpy loss resulting in ΔG° becoming slightly more negative relative to the single mutants (Table 1). Hence the dissociation constant of the CK2$\alpha^{1-335,Leu41Ala,Phe54Ala}$ mutant (K_D = 234.74 nM) was smaller than those of the single mutants.

Gel Filtration and in Vitro Pull-Down Studies. We performed gel filtration analyses to probe whether the loss of affinity to CK2β results in a reduced ability of the CK2α mutants to form the typical heterotetrameric CK2 holoenzyme (Figure 1A). Five different samples, each of which contains the same amount of CK2β^{1-193} mixed with excess amounts of the five CK2α constructs, were applied to the gel filtration column (Figure 4A). Significant peaks of chromatograms were analyses by SDS−PAGE (Figure 4B).

The chromatogram for the wild-type mixture (CK2α^{1-335} plus CK2β^{1-193}; red curve in Figure 4A) serves as a reference: it shows two peaks corresponding to 142 and 44 kDa, which roughly coincides with the expected molecular masses of 125 kDa for the holoenzyme and 40 kDa for the free catalytic subunit. Any unbound CK2β^{1-193} dimers with a theoretical molecular mass of 45 kDa should elute together with free CK2α^{1-335}, but an SDS−PAGE analysis (lanes 2 and 7 of Figure 4B) confirms that CK2β^{1-193} is completely integrated in the tetrameric holoenzyme.

The mixture with the high-affinity mutant CK2$\alpha^{1-335,Ile69Ala}$ behaves the same as the reference (Figure 4A, green line; lanes 3 and 8 of Figure 4B), but significant changes are observed with the three low-affinity mutants CK2$\alpha^{1-335,Leu41Ala}$, CK2$\alpha^{1-335,Phe54Ala}$, and CK2$\alpha^{1-335,Leu41Ala,Phe54Ala}$ (blue, magenta, and black lines in Figure 4A). With each of these mutants interaction and aggregation products occur in the high molecular fractions around 14 and 15 mL; nevertheless, none them shows the normal holoenzyme peak at the expected elution volume. However, the mutants CK2$\alpha^{1-335,Leu41Ala}$ and CK2$\alpha^{1-335,Phe54Ala}$ are insofar similar to the wild-type CK2α^{1-335} as their low molecular fractions are free from unbound CK2β^{1-193} (lanes 9 and 10 of Figure 4B) and as they produce maxima around 14.5 mL (peak 2 in Figure 4A) with apparently the same CK2β^{1-193} content as the holoenzyme (lanes 4 and 5 of Figure 4B). The apparent molecular mass of these aggregates (110 kDa) does not fit to a defined stoichiometry.

In the case of the double mutant CK2$\alpha^{1-335,Leu41Ala,Phe54Ala}$ even peak 2 is absent. Instead, a shallow maximum around 15 mL occurs (peak 3; black line of Figure 4A) which, however, does not contain CK2β^{1-193} in significant amounts (lane 6 of Figure 4B). Rather CK2β^{1-193} appears in the fractions of the free CK2$\alpha^{1-335,Leu41Ala,Phe54Ala}$ subunit.

We then set out to complement our results by performing an *in vitro* interaction study using GST-tagged CK2α wild type and the same mutants used for ITC measurements adhered to glutathione−agarose beads. We incubated each CK2α variant with increasing concentrations of CK2β in harsh buffer conditions to determine the extent of binding to each. Immunoblotting using antibodies specific for GST and CK2β revealed that for the highest amount of His-CK2β added (2.4 μg/mL) 86 times less CK2β was detectable in the case of the Leu41Ala mutant and 355 times less for the Phe54Ala mutant, when compared to the interaction between the wild-type CK2 proteins (Figure 4C). In the case of the Leu41Ala,Phe54Ala double mutant there was 159 times less CK2β that had been pulled down. For the Ile69Ala

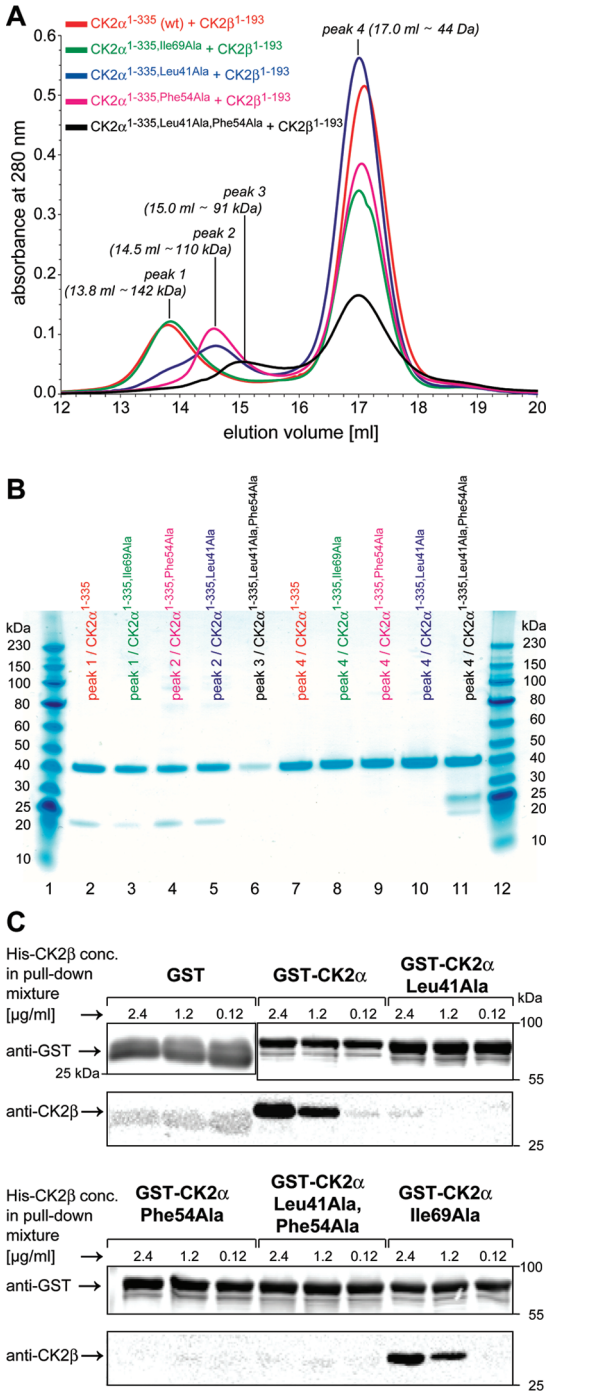

FIGURE 4: Supplementary *in vitro* interaction analysis between CK2α and CK2β constructs. (A) Gel filtration experiments with mixtures of CK2β^{1-193} and excess amounts of the following CK2α variants: CK2α^{1-335} (red), CK2$\alpha^{1-335,Leu41Ala}$ (blue), CK2$\alpha^{1-335,Phe54Ala}$ (magenta), CK2$\alpha^{1-335,Ile69Ala}$ (green), and CK2$\alpha^{1-335,Leu41Ala,Phe54Ala}$ (black). The individual runs were performed under identical conditions, and the resulting chromatograms were finally superimposed. (B) SDS−PAGE of the gel filtration runs shown in panel A of the figure. The peak numbers refer to the chromatograms in panel A. (C) Immunoblot analysis of *in vitro* pull-down experiments with glutathione−agarose beads. GST-tagged CK2α variants or GST as a negative control was coupled to the glutathione−agarose beads and incubated with 2.4, 1.2, or 0.12 μg/mL CK2β. After careful washing and SDS−PAGE, immunoblotting using antibodies specific for GST and CK2β revealed first the successful binding of the GST-CK2α fusion proteins to the beads and second the amount of CK2β coprecipitated due to an interaction with the respective CK2α construct. The anti-CK2β antibody shows a little cross-reaction with GST. Numbers on the right and left indicate the sizes of nearby marker bands.

single mutation we detected an amount of CK2β that was most comparable to the interaction of the wild-type CK2 proteins (3 times less).

Thermostability and Catalytic Activity of the CK2α Variants. We were then interested in the question whether mutations at the CK2β interface of CK2α affect the general enzymological profile of the catalytic subunit. First, we tested the thermostability with differential scanning calorimetry (DSC) and observed the tendency that the removal of hydrophobic side chains from the interaction interface results in a decrease of the melting temperature T_m (Figure 5). The replacement of Ile69 had the smallest impact (T_m = 41.3 °C) compared to 45.6 °C for the CK2α$^{1-335}$ construct, whereas CK2α$^{1-335,Leu41Ala}$ has an unfolding temperature of 40.0 °C and CK2α$^{1-335,Phe54Ala}$ unfolded at 38.3 °C. The low solubility of CK2α$^{1-335,Leu41Ala,Phe54Ala}$ prevented a successful DSC scan, but it is, in particular combined with our observation of an increased tendency of this mutant to precipitate at temperatures higher than 30 °C, a qualitative indication for a significantly reduced thermostability.

Finally, the CK2α mutants were characterized employing Michaelis–Menten kinetics with respect to the cosubstrate ATP (Figure 6), and from these the critical parameters K_M and k_{cat} were derived (Table 2). The three single mutants were, as measured by the k_{cat}/K_M ratios (Table 2), only slightly less active than CK2α$^{1-335}$. For the double mutant CK2α$^{1-335,Leu41Ala,Phe54Ala}$, however, we observed a fairly low activity even at a high ATP concentration (200 μM) with the method used. Therefore, for CK2α$^{1-335,Leu41Ala,Phe54Ala}$ we measured the activity only under presumable saturation conditions and took this activity as maximal velocity v_{max}; the k_{cat} value derived from this v_{max} was about 10 times reduced compared to the wild-type CK2α$^{1-335}$ (Table 2).

To check whether the conspicuously reduced activity of CK2α$^{1-335,Leu41Ala,Phe54Ala}$ can be rescued with CK2β, we performed a series of activity assays under saturation conditions for casein and ATP and with increasing concentrations of CK2β^{1-193} up to a final molar excess of 5. A further deviation from the assay protocol described above was the presence of 300 mM NaCl; it was motivated by the early finding of Grankowski et al. (*32*) that the CK2 holoenzyme, rather than the free CK2α subunit, possesses an activity maximum at such a salt concentration. Under these conditions we observed that CK2β^{1-193} increased the activity of CK2α$^{1-335}$ up to a limiting factor of 2.2, which was reached when an equimolar ratio between CK2α$^{1-335}$ and CK2β^{1-193} was obtained. In contrast, CK2β^{1-193} did not stimulate CK2α$^{1-335,Leu41Ala,Phe54Ala}$, not even with a 5-fold molar excess.

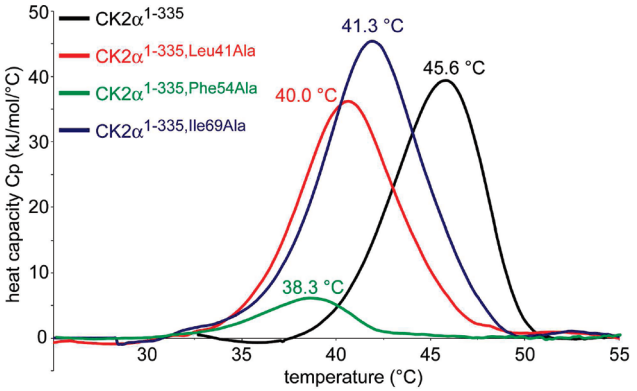

FIGURE 5: Differential scanning calorimetry (DSC) with various CK2α$^{1-335}$ mutants. For each protein variant three independent DSC runs were performed. One representative curve of each triple is shown. The unfolding temperatures given in the figure are averages of three experiments.

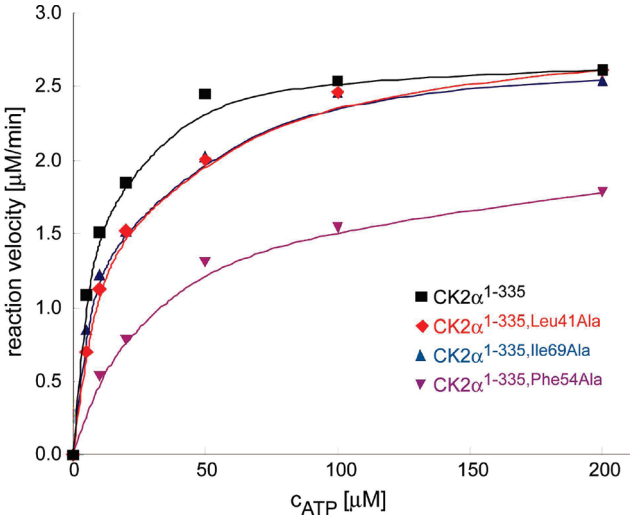

FIGURE 6: Michaelis–Menten plots of the reaction kinetics of CK2α$^{1-335}$ and the mutants CK2α$^{1-335,Leu41Ala}$, CK2α$^{1-335,Phe54Ala}$, and CK2α$^{1-335,Ile69Ala}$ at 30 °C.

DISCUSSION

Temperature Independence of the CK2α/CK2β Interaction. An interesting detail of the calorimetric studies that we present here was the fact that the affinity between CK2α and CK2β was temperature-independent in the range between 20 and 35 °C due to an entropy/enthalpy compensation (Figure 2A). This observation (and its extrapolation to higher and lower temperatures) means that the CK2 holoenzyme possesses an architecture of significant thermal stability. Our result seems consistent with a recent report that CK2 plays a critical role in circadian temperature compensation in *Neurospora crassa* (*33*).

Structure-Based Modeling of Thermodynamic Data. The protonation independence of the CK2α/CK2β binding reaction (Figure 2B) and even more the significantly negative standard heat capacity change of about −1.3 kJ/(mol·K) that we determined from the temperature-dependent thermodynamic profile (Figure 2A) are consistent with a strong hydrophobic character of the interaction (*34*, *35*) and with the accumulation of hydrophobic side chains in the contact region (Figure 1).

For a quantitative analysis we computed changes of solvent-accessible surface areas of ΔASA_{ap} = 1027 Å^2 and ΔASA_{pol} = 573 Å^2 (see Experimental Procedures for details). These values were applied to the temperature-corrected equations of Holdgate et al. (*29*). They lead to a theoretical ΔC_p of −1.26 kJ/(mol·K) which coincides well with experimental value. However, the further calculated thermodynamic parameters were as follows: $\Delta H°$ = 10.4 kJ/mol; $-T\Delta S°$ = −99.2 kJ/mol; $\Delta G°$ = −88.7 kJ/mol. In other words, a high affinity between CK2α and CK2β can be theoretically rationalized from the CK2 holoenzyme structure, but it should depend mostly on the entropic instead of the enthalpic term in contrast to our experimental data (Table 1). We tested an alternative parametrization that had been successfully applied for a protein/protein interaction (*36*), but the central result, a strong underestimation of the enthalpic contribution to $\Delta G°$, was similar.

Table 2: Kinetic Parameters of Some Human CK2α Variants

mutant	v_{max} (μM/min)	$K_{M,ATP}$ (μM)	k_{cat} (min^{-1})	$k_{cat}/K_{M,ATP}$ (min^{-1} μM^{-1})
CK2α$^{1-335}$ (wt)	6.62	10.09	12.47	1.14
CK2α$^{1-335,Leu41Ala}$	4.55	12.73	8.97	0.70
CK2α$^{1-335,Phe54Ala}$	4.35	11.00	8.63	0.78
CK2α$^{1-335,Leu41Ala,Phe54Ala}$	0.59	nd	1.25	nd
CK2α$^{1-335,Ile69Ala}$	3.33	21.33	6.04	0.28

This deviation between experiment and modeling is insofar not unexpected as the latter depends on a rigid-body approximation, i.e., the assumption that no conformational changes occur during the association of CK2α and CK2β. This simplification is largely true for CK2β (*30*), at least for the construct CK2β^{1-193} that we used for this study, but for human CK2α an opening motion of the β4/β5 loop as illustrated in the zoom area of Figure 1A is required. This conformational change together with its consequences for the nearby solvent and protein structure is a candidate source of the strong enthalpic signal associated with the CK2α/CK2β interaction. However, to present computational evidence for this hypothesis is difficult since current modeling techniques do not allow an estimate of the impact of such conformational effects on the thermodynamic functions quantitatively with reasonable accuracy.

Key Residues in the Subunit Interface. Definitely the β4/β5 loop motion in CK2α has an influence on the solvent accessibility of the neighboring interaction surface and its hydrophobic side chains (Figure 1A). This was demonstrated by a computational quantification that we performed for the three mutated residues (Leu41, Phe54, and Ile69) with AREAIMOL (*26*) pursuing the interaction path from state 1 (monomeric CK2α with closed β4/β5 loop) over state 2 (monomeric CK2α with open β4/β5 loop) to state 3 (CK2β-bound CK2α with open β4/β5 loop). For state 1 we took a highly resolved structure of monomeric CK2α$^{1-335}$ with a well-defined β4/β5 loop [(3BQC (*37*)]; state 2 has as yet never been structurally observed with human CK2α so we constructed it by isolating CK2α subunit A from the CK2 holoenzyme structure (*6*); finally, state 3 was the CK2α subunit A within the CK2 holoenzyme. The resulting solvent accessibilities were as follows: Leu41, 74.0 Å^2 (state 1) → 101.8 Å^2 (state 2) → 19.4 Å^2 (state 3); Phe54, 26.6 Å^2 (state 1) → 45.4 Å^2 (state 2) → 1.2 Å^2 (state 3); Ile69, 18.6 Å^2 (state 1) → 42.9 Å^2 (state 2) → 19.0 Å^2 (state 3).

Thus, during the complete assembly path the solvent-exposed surface of all three residues runs over a maximum (state 2); a significant reduction, however (ASA difference between state 1 and state 3), occurs only for Leu41 and Phe54 but not for Ile69. This result correlates well with the $\Delta\Delta G°$ values of the alanine scanning experiment (Table 1) that identified Leu41 and Phe54 but not Ile69 as interaction "hot spots" as defined by Bogan and Thorn (*2*).

A look at the molecular surfaces is also instructive for a rationalization of the somewhat surprising ITC result that the double mutant CK2α$^{1-335,Leu41Ala,Phe54Ala}$ retains an affinity to CK2β^{1-193} that is, as measured by the $\Delta G°$ values (Table 1), in the same order of magnitude as that of the single mutants CK2α$^{1-335,Leu41Ala}$ and CK2α$^{1-335,Phe54Ala}$. The side chains of Leu41 and Phe54 are closely packed to one another as Figure 1C illustrates and as an AREAIMOL (*26*) calculation of the contact surfaces underlines quantitatively. If one defines either the Leu41 side chain or the Phe54 side chain as a pseudoligand, each of the other side chains is that part of the CK2α$^{1-335}$ structure with the largest contact surface (18.7 Å^2 on average). As a consequence the two side chains are not independent of each other; rather they form a block that moves upon CK2β binding concertedly in the direction of its novel contact partner Met169 of CK2β (Figure 1C) whereas Ile69 only changes the side chain rotamer but keeps its position. Hence, a removal of the Leu41/Phe54 block has more or less the same effect as either of the single mutations.

Since no 3D structures of the CK2α mutants exist so far, it remains an open question how the conformations of neighboring regions critical for the interaction with CK2β are affected by the mutations. It is possible for example that the unbound low-affinity mutants CK2α$^{1-335,Leu41Ala}$, CK2α$^{1-335,Phe54Ala}$, and CK2α$^{1-335,Leu41Ala,Phe54Ala}$ no longer prefer state 1 as wild-type human CK2α but state 2, i.e., that they preferentially exist with an open β4/β5 loop as is known for maize CK2α (*38*). It is also possible that in the point mutants CK2α$^{1-335,Leu41Ala}$ and CK2α$^{1-335,Phe54Ala}$ the remaining side chain of the Leu41/Phe54−block adopts, after loss of its stabilizing counterpart, an alternative conformation less favorable for the interaction with CK2β.

While a comprehensive structural and computational rationalization of the ITC results is not possible in the moment, they correlate reasonably with the outcome of the two other interaction-dependent experimental techniques applied here:

(1) The GST pull-down interaction studies (Figure 4C) show, bearing in mind the semiquantitative character of this method, that the interactions of the CK2 subunits are disturbed to different extents for all of the mutants except the Ile69Ala substitution and hence correspond to what was observed using ITC.

(2) In gel filtration a CK2β^{1-193} mixture with the high-affinity mutant CK2α$^{1-335,Ile69Ala}$ has a normal run behavior in comparison to the wild type whereas mixtures with the three low-affinity mutants have not (Figure 4A). In particular, the double mutant CK2α$^{1-335,Leu41Ala,Phe54Ala}$ shows no evidence of an interaction with CK2β^{1-193} under these conditions. One reason for this finding may be the reduced run temperature (10 °C) which disfavors the entropic term that dominates the binding $\Delta G°$ for this mutant (Figure 3F). Moreover, the kinetic instability of a protein/protein complex can affect the results of a dynamic technique like gel filtration. In case of a high rate constant the dissociation reaction can compete with the separation of the particles at the gel pores. As a consequence protein/protein oligomers either decompose or are at least significantly retarded during a gel filtration run. Possibly the latter happened for CK2α$^{1-335,Leu41Ala}$/CK2β^{1-193}, and CK2α$^{1-335,Phe54Ala}$/CK2β^{1-193}, complexes that eluted 0.7 mL later than the normal CK2 holoenzyme particles (blue and magenta lines in Figure 4A). In case this kinetic interpretation is correct, the dissociation rate constants of the corresponding interactions should be significantly higher than 3.6×10^{-4} s^{-1}, which is the value determined by surface plasmon resonance for wild-type constructs of CK2α and CK2β (*18*).

Table 3: Final Overview of CK2α Variants[a]

mutant	interaction capability with CK2β: ITC: $K_{D,wt}/K_{D,mut}$	interaction capability with CK2β: pull down assay: CK2β signal$_{mut}$/ CK2β signal$_{wt}$	interaction capability with CK2β: gel filtration: CK2α/CK2β complex stability	loss of thermostability $T_{m,wt} - T_{m,mut}$ (°C)	relative catalytic efficiency $(k_{cat}/K_M)_{mut}/(k_{cat}/K_M)_{wt}$
$CK2\alpha^{1-335}$ (wt)	1.000	1.000	high	0	1
$CK2\alpha^{1-335,Leu41Ala}$	0.010	0.012	low	5.6	0.61
$CK2\alpha^{1-335,Phe54Ala}$	0.012	0.003	low	7.3	0.68
$CK2\alpha^{1-335,Leu41Ala,Phe54Ala}$	0.016	0.006	very low	(probably high)	(very low)
$CK2\alpha^{1-335,Ile69Ala}$	0.256	0.333	high	4.3	0.25

[a] T_m: melting point.

Final Evaluation of the CK2α Mutants. Even more interesting than a comprehensive structure-based physical understanding of the interaction defects of the CK2α mutants will be the question whether they will show phenotypic effects after transfection of cells. The "ideal" mutant for such studies is no longer competent to interact with CK2β but has preserved the remaining characterics of wild-type CK2α. For a final evaluation of our CK2α mutants Table 3 summarizes the basic findings obtained in this study. According to these data $CK2\alpha^{1-335,Ile69Ala}$ is not a candidate due to its still strong affinity to CK2β. On the other hand, the double mutant $CK2\alpha^{1-335,Leu41Ala,Phe54Ala}$ must be rejected because of its stability problems and in particular because of its marginal catalytic activity that could not even be recovered by a large excess of $CK2\beta^{1-193}$.

The remaining candidates are the mutants $CK2\alpha^{1-335,Leu41Ala}$ and $CK2\alpha^{1-335,Phe54Ala}$ in which one of two side chains identified here as interaction "hot spots" is removed. Transfection studies with these mutants might be valuable to probe the importance of the CK2α/CK2β interaction in a cellular context and thus to validate the qualification of this interaction as a pharmacological target.

REFERENCES

1. Prudent, R., and Cochet, C. (2009) New protein kinase CK2 inhibitors: jumping out of the catalytic box. *Chem. Biol. 16*, 112–120.
2. Bogan, A. A., and Thorn, K. S. (1998) Anatomy of hot spots in protein interfaces. *J. Mol. Biol. 280*, 1–9.
3. Guerra, B., and Issinger, O.-G. (2008) Protein kinase CK2 in human diseases. *Curr. Med. Chem. 15*, 1870–1886.
4. Battistutta, R. (2009) Protein kinase CK2 in health and disease: structural bases of protein kinase CK2 inhibition. *Cell. Mol. Life Sci. 66*, 1868–1889.
5. Duncan, J. S., Gyenis, L., Lenehan, J., Bretner, M., Graves, L. M., Haystead, T. A., and Litchfield, D. W. (2008) An unbiased evaluation of CK2 inhibitors by chemoproteomics: characterization of inhibitor effects on CK2 and identification of novel inhibitor targets. *Mol. Cell Proteomics 7*, 1077–1088.
6. Niefind, K., Guerra, B., Ermakowa, I., and Issinger, O.-G. (2001) Crystal structure of human protein kinase CK2: insights into basic properties of the CK2 holoenzyme. *EMBO J. 20*, 5320–5331.
7. Allende, J. E., and Allende, C. C. (1995) Protein kinases. 4. Protein kinase CK2: an enzyme with multiple substrates and a puzzling regulation. *FASEB J. 9*, 313–323.
8. Issinger, O.-G., Brockel, C., Boldyreff, B., and Pelton, J. T. (1992) Characterization of the α and β subunits of casein kinase 2 by far-UV CD spectroscopy. *Biochemistry 31*, 6098–6103.
9. Meggio, F., Boldyreff, B., Marin, O., Pinna, L. A., and Issinger, O.-G. (1992) Role of the β subunit of casein kinase-2 on the stability and specificity of the recombinant reconstituted holoenzyme. *Eur. J. Biochem. 204*, 293–297.
10. Ruzzene, M., and Pinna, L. A. (2009) Addiction to protein kinase CK2: a common denominator of diverse cancer cells? *Biochim. Biophys. Acta 1804*, 499–504.
11. Ahmed, K., Gerber, D. A., and Cochet, C. (2002) Joining the cell survival squad: an emerging role for protein kinase CK2. *Trends Cell Biol. 12*, 226–230.
12. Desagher, S., Osen-Sand, A., Montessuit, S., Magnenat, E., Vilbois, F., Hochmann, A., Journot, L., Antonsson, B., and Martinou, J. C. (2001) Phosphorylation of Bid by casein kinases I and II regulates its cleavage by caspase 8. *Mol. Cell 8*, 601–611.
13. St-Denis, N. A., and Litchfield, D. W. (2009) Protein kinase CK2 in health and disease: from birth to death: the role of protein kinase CK2 in the regulation of cell proliferation and survival. *Cell. Mol. Life Sci. 66*, 1817–1829.
14. Scaglioni, P. P., Yung, T. M., Cai, L. F., Erdjument-Bromage, H., Kaufman, A. J., Singh, B., Teruya-Feldstein, J., Tempst, P., and Pandolfi, P. P. (2006) A CK2-dependent mechanism for degradation of the PML tumor suppressor. *Cell 126*, 269–283.
15. Di Maira, G., Brustolon, F., Bertacchini, J., Tosoni, K., Marmiroli, S., Pinna, L. A., and Ruzzene, M. (2007) Pharmacological inhibition of protein kinase CK2 reverts the multidrug resistance phenotype of a CEM cell line characterized by high CK2 level. *Oncogene 26*, 6915–6926.
16. Di Maira, G., Brustolon, F., Tosoni, K., Belli, S., Krämer, S. D., Pinna, L. A., and Ruzzene, M. (2008) Comparative analysis of CK2 expression and function in tumor cell lines displaying sensitivity vs. resistance to chemical induced apoptosis. *Mol. Cell. Biochem. 316*, 155–161.
17. Salvi, M., Sarno, S., Marin, O., Meggio, F., Itarte, E., and Pinna, L. A. (2006) Discrimination between the activity of protein kinase CK2 holoenzyme and its catalytic subunits. *FEBS Lett. 580*, 3948–3952.
18. Martel, V., Filhol, O., Nueda, A., and Cochet, C. (2002) Dynamic localization/association of protein kinase CK2 subunits in living cells: a role in its cellular regulation? *Ann. N.Y. Acad. Sci. 973*, 272–277.
19. Filhol, O., Nueda, A., Martel, V., Gerber-Scokaert, D., Benitez, M. J., Souchier, C., Saoudi, Y., and Cochet, C. (2003) Live cell fluorescence imaging reveals the dynamics of protein kinase CK2 individual subunits. *Mol. Cell. Biol. 23*, 975–987.
20. Laudet, B., Barrette, C., Dulery, V., Renaudet, O., Dumy, P., Metz, A., Prudent, R., Deshire, A., Dideberg, O., Filhol, O., and Cochet, C. (2007) Structure-based design of small peptide inhibitors of protein kinase CK2 subunit interaction. *Biochem. J. 408*, 363–373.
21. Raaf, J., Brunstein, E., Issinger, O.-G., and Niefind, K. (2008) The CK2a/CK2ss interface of human protein kinase CK2 harbors a binding pocket for small molecules. *Chem. Biol. 15*, 111–117.
22. Laudet, B., Moucadel, V., Prudent, R., Filhol, O., Yung-Sing Wong, Y.-S., Daniel Royer, D., and Cochet, C. (2008) Identification of chemical inhibitors of protein-kinase CK2 subunit interaction. *Mol. Cell. Biol. 316*, 63–69.
23. Ermakova, I., Boldyreff, B., Issinger, O.-G., and Niefind, K. (2003) Crystal structure of a C-terminal deletion mutant of human protein kinase CK2 catalytic subunit. *J. Mol. Biol. 330*, 925–934.
24. Boldyreff, B., Meggio, F., Pinna, L. A., and Issinger, O.-G. (1993) Reconstitution of normal and hyperactivated forms of casein kinase-2 by variably mutated β-subunits. *Biochemistry 32*, 12672–12677.
25. Roskosko, R., Jr. (1983) Assays of protein kinase. *Methods Enzymol. 99*, 3–6.
26. Collaborative Computational Project, Number 4 (1994) The CCP4 suite: programs for protein crystallography. *Acta Crystallogr. D50*, 760–763.
27. Perozzo, R., Folkers, G., and Scapozza, L. (2004) Thermodynamics of protein-ligand interactions: history, presence, and future aspects. *J. Recept. Signal Transduct. 24*, 1–52.
28. Gómez, J., and Freire, E. (1995) Thermodynamic mapping of the inhibitor site of the aspartic protease endothiapepsin. *J. Mol. Biol. 252*, 337–350.

29. Holdgate, G. A., Tunnicliffe, A., Ward, W. H., Weston, S. A., Rosenbrock, G., Barth, P. T., Taylor, I. W., Pauptit, R. A., and Timms, D. (1997) The entropic penalty of ordered water accounts for weaker binding of the antibiotic novobiocin to a resistant mutant of DNA gyrase: a thermodynamic and crystallographic study. *Biochemistry 36*, 9663–9673.
30. Raaf, J., Brunstein, E., Issinger, O.-G., and Niefind, K. (2008) The interaction of CK2α and CK2*β*, the subunits of protein kinase CK2, requires CK2*β* in a pre-formed conformation and is enthalpically driven. *Protein Sci. 17*, 2180–2186.
31. Goldberg, R. N., Kishore, N., and Lennen, R. M. (2002) Thermodynamic quantities for the ionization reactions of buffers. *J. Phys. Chem. Ref. Data 31*, 231–370.
32. Grankowski, N., Boldyreff, B., and Issinger, O. G. (1991) Isolation and characterization of recombinant human casein kinase II subunits α and *β* from bacteria. *Eur. J. Biochem. 198*, 25–30.
33. Mehra, A., Shi, M., Baker, C. L., Colot, H. V., Loros, J. J., and Dunlap, J. C. (2009) A role for casein kinase 2 in the mechanism underlying circadian temperature compensation. *Cell 137*, 749–760.
34. Sturtevant, J. M. (1977) Heat capacity and entropy changes in processes involving proteins. *Proc. Natl. Acad. Sci. U.S.A. 74*, 2236–2240.
35. Spolar, R. S., Ha, J. H., and Record, M. T., Jr. (1989) Hydrophobic effect in protein folding and other noncovalent processes involving proteins. *Proc. Natl. Acad. Sci. U.S.A. 86*, 8382–8385.
36. Baker, B. M., and Murphy, K. P. (1997) Dissecting the energetics of a protein-protein interaction: the binding of ovomucoid third domain to elastase. *J. Mol. Biol. 268*, 557–569.
37. Raaf, J., Klopffleisch, K., Issinger, O.-G., and Niefind, K. (2008) The catalytic subunit of human protein kinase CK2 structurally deviates from its maize homologue in complex with the nucleotide competitive inhibitor emodin. *J. Mol. Biol. 377*, 1–8.
38. Niefind, K., Guerra, B., Pinna, L. A., Issinger, O.-G., and Schomburg, D. (1998) Crystal structure of the catalytic subunit of protein kinase CK2 from *Zea mays* at 2.1 Å resolution. *EMBO J. 17*, 2451–2462.
39. Esnouf, R. M. (1997) An extensively modified version of MolScript that includes greatly enhanced coloring capabilities. *J. Mol. Graphics 15*, 132–134.
40. Merritt, E. A., and Bacon, D. J. (1997) Raster3D: photorealistic molecular graphics. *Methods Enzymol. 277*, 505–524.
41. DeLano, W. L. The PyMOL Molecular Graphics System, DeLano Scientific LLC, San Carlos, CA.
42. Schomburg, D., and Reichelt, J. (1988) BRAGI: a comprehensive protein modeling program system. *J. Mol. Graphics 6*, 161–165.